Tuning the Double Layer of Graphene Oxide through Phosphorus Doping for Enhanced Supercapacitance

Weixin Song,[1,3] Johannes Lischner,[1,2,3] Victoria G. Rocha,[1,4] Heng Qin,[1,3] Jiahui Qi,[1,3] Joseph H.L. Hadden,[1,3] Cecilia Mattevi,[1,3] Fang Xie,[1,3] D. Jason Riley[1,3]*

1 Department of Materials, Imperial College London, London SW7 2AZ, U.K.

2 Thomas Young Centre at Imperial College London, London SW7 2AZ, U.K.

3 London Centre for Nanotechnology, London SW7 2AZ, U.K.

4 School of Engineering, Cardiff University, Cardiff CF24 3AA, U.K.

ABSTRACT: The electrochemical double layer plays a fundamental role in energy storage applications. Control of the distribution of ions in the double layer at the atomistic scale offers routes to enhanced material functionality and device performance. Here we demonstrate how the addition of an element from the third row of the periodic table, phosphorus, to graphene oxide increases the measured capacitance and present density functional theory calculations that relate the enhanced charge storage to structural changes of the electrochemical double layer. Our results point to how rational design of materials at the atomistic scale can lead to improvements in their performance for energy storage.

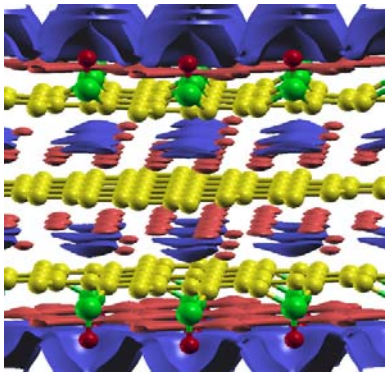

In an Electrochemical Double Layer Capacitor (EDLC) charge is stored in the ionic double layer formed between the solid substrate and the liquid electrolyte. This mechanism of interfacial charge storage leads to high discharge rates and excellent recyclability. To maximise the capacitance of EDLC devices conductive materials of high specific area are employed as electrodes. Graphene with its high surface area to volume ratio, low density and remarkable electronic, mechanical and thermal properties has been shown to be a suitable electrode material in EDLCs[1, 2]. Heteroatomic doping into graphene, which is also called surface functionalization, is a promising method of tuning the physicochemical and electronic properties of the material. Heteroatoms such as nitrogen (N), oxygen (O), phosphorus (P), boron (B) and sulphur (S) yield functional groups on the surface of graphene and introduce defects into the lattice[3]. Heteroatomic doping not only helps maintain the layer separation but also alters the electron distribution in the graphene layer, provides sites for specific adsorption and may yield redox active surface entities that can enhance the specific capacitance of the electrodes.

Graphene oxide (GO), oxygen-functionalized graphene, is formed when graphene is exfoliated from graphite in strong acids. A range of oxygen functional groups, including hydroxyl, epoxy, carboxyl, phenol, carbonyl and quinone, have been identified on the surface of GO[4]. The enriched oxygen functional groups play important roles in the electrochemical capacitive performance of chemically functionalized graphene in electrolytes of different p*H* and provide abundant covalent bonding sites for further functionalization with other atoms. Specific capacitances as high as 189 F g^{-1} and 348 F g^{-1} have been reported for GO[5] and reduced graphene oxide (rGO)[6, 7], respectively. rGO is typically formed by reducing GO with hydrazine or a hydrogen plasma or thermal treatment during processing. Electron-rich nitrogen (N) doping has been widely used to improve the electronic conductivity and catalytic activity of graphene[8]. Pyridinic N (N-6), pyrrolic N (N-5) and graphitic sp^2 N (N-Q) are formed when nitrogen replaces carbon atoms in the graphene[9]. Capacitances as high as 287 F g^{-1} have been reported for nitrogen doped graphene[10].

Phosphorus (P) is located in the same main group (15) as N and has the same number of valence electrons. The electronegativity of P atoms (2.19) is lower than that of C atoms (2.55), so P will be partially positively charged in the C-P bond and the polarity of the C-P bond is opposite to that of C-N bond. Moreover, the larger radius of a P atom relative to a C atom will lead to structural distortions of the hexagonal carbon framework with P protruding out of the graphene plane due to the longer P-C bond as compared with the C-C[11] bond and could result in increased surface area and improved separation of the graphene layers. Recently, P-doped carbon materials have been proposed for use in supercapacitors, batteries, field-effect transistors and catalysts for oxygen reduction reaction (ORR)[12, 13,14]. To date the amount of P incorporated on graphene oxide has been low, typically <3%. In this work highly P-doped graphene oxide (PGO) with doping levels exceeding 7% was prepared. It is demonstrated that high P doping results in an increased specific capacitance of PGO and improved cycling performance. Density functional theory (DFT) calculations are employed to investigate the structure of PGO and simulate the ion distribution at the PGO-electrolyte interface to explain the enhanced capacitance.

Table 1. C, O and P content of P-doped graphene oxide from XPS analysis and corresponding ratio of P:C and O:C.

Label	C (%)	O (%)	P (%)	P:C	O:C
GO	68.17	31.83	-	-	0.467
$PGO_{1TPA+1.3TOP,\ 800}$	60.85	31.38	7.77	0.128	0.516
$PGO_{1TPA+1.3TOP,\ 900}$	93.50	4.19	2.31	0.025	0.045
$PGO_{1TPA,\ 800}$	94.73	3.51	1.76	0.019	0.037
$PGO_{1TPA,\ 900}$	96.42	2.43	1.14	0.012	0.025
$PGO_{4TPA,\ 800}$	90.90	6.61	2.49	0.027	0.073
$PGO_{7TPA,\ 800}$	62.93	26.88	10.19	0.162	0.427
$PGO_{1.3TOP,\ 800}$	94.63	3.70	1.68	0.018	0.039
$PGO_{1.3TBP,\ 800}$	92.63	5.97	1.40	0.015	0.064
$PGO_{0.7TOP,\ 800}$	96.34	3.10	0.55	0.006	0.032
$PGO_{0.7TOP,\ 900}$	92.19	5.60	2.20	0.024	0.061

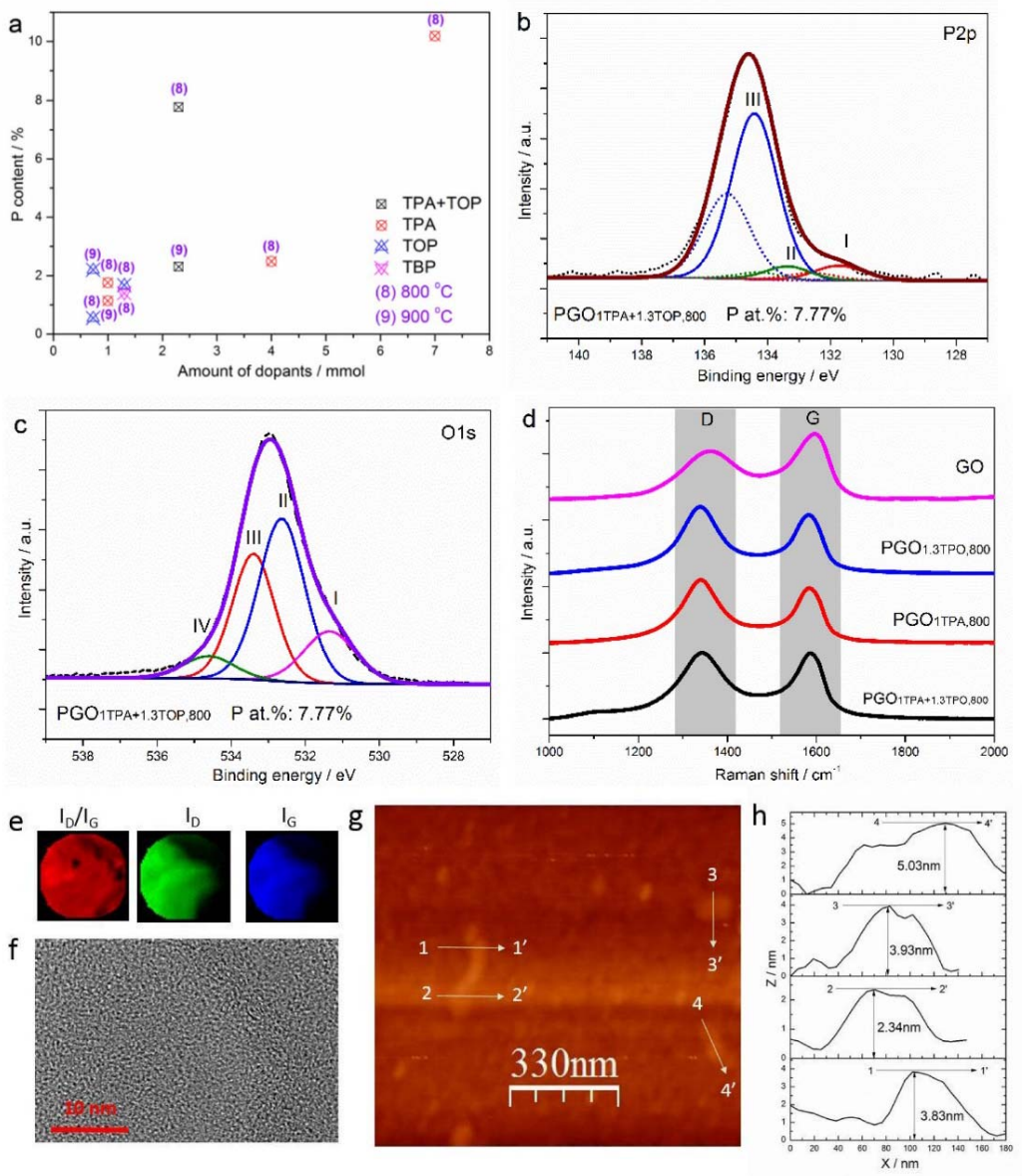

Fig. 1 Characterization of P-doped graphene oxide. (a) Relationship between P content (at.%) of the product and the amount of P source (mmol) for doping 67 mg GO at 800 and 900 °C. (b) P2p and (c) O1s high-resolution XPS spectra of the as-prepared $PGO_{1TPA+1.3TOP,800}$. The corresponding bonds for P2p analysis are P-C (I), P=O/P-O-P (II), P-O (III) and for O1s are C=O and P=O (I), -O- (II), P-O-H (III), absorbed H_2O and O_2 (IV). (d) Raman spectra of GO, $PGO_{1TPA+1.3TOP,800}$, $PGO_{1TPA,\ 800}$ and $PGO_{1.3TOP,\ 800}$. (e) Raman mapping of the D-band to G-band intensity ratio (I_D/I_G), I_D and I_G. (f) TEM images of $PGO_{1TPA+1.3TOP,800}$. (g) AFM image of $PGO_{1TPA+1.3TOP,800}$ and (h) the measured thickness in (g) in the denoted directions.

P Doping in Graphene Oxide. To dope the GO three sources of phosphorus: tri-n-octylphosphine (TOP), tri-n-butylphosphine (TBP) and tetradecylphosphonic acid (TPA) and two annealing temperatures (800°C and 900°C) were investigated. 0.7 mmol to 7 mmol of TOP, TBP and/or TPA were added to 10 mL of a 6.7 g dm^{-3} aqueous suspension of GO, the annealed samples are labelled as $PGO_{xPS,T}$ where x is the number of mmol of the phosphorus source (PS) used and T is the annealing temperature. The atomic percentages of C, O and P in the GO and as-prepared PGO samples was determined by X-ray photoelectron spectrum (XPS), see Fig. S1. The measured P:C and O:C ratios for GO and PGO samples are presented in Table 1.

The XPS data shows that in all samples the percentage of O is greater than that of P. In those samples of which the amount of P incorporated in the gaphene is <3%, the O:C ratio is significantly lower than that of the parent GO. Both the heat and P sources acting as

reducing agents at high temperature contribute to the oxygen reduction (O/C ratios of GO treated at 800 and 900 °C are listed in Table S2). Comparison of the elemental composition of the samples $PGO_{1.3TOP,\ 800}$ and $PGO_{1.3TBP,\ 800}$ suggests that TBP is a poorer reducing agent than TOP and less efficient at P-doping the GO. Studies performed at different annealing temperatures show that for TOP an increase in annealing temperature favours P doping whilst for TPA and the mixed TOP-TPA system P doping is enhanced at the lower temperature. For synthesis using a single source of P the amount of P in the final material increases with the number of mmol of P sources, see Fig. 1a. When 7 mmol of TPA are added to 67 mg of GO and annealed at 800°C, a P-doping level of 10.19% is achieved, considerably greater than values previously reported in the literature[3, 12, 13, 15].

7.77% P-doping can be achieved using only 2.3 mmol of P sources when a mixed system is used, 1 mmol TPA with 1.3 mmol TOP, pointing to a synergistic effect in this mixed source system, see Fig. 1a. To investigate why the mixed TPA-TOP system leads to more efficient doping of the GO, XRD studies were performed on GO and GO plus P precursor systems prior to high temperature annealing. The GO was mixed with measured quantities of surfactant, the system dried at temperatures of 60°C, 120°C and 180°C for 12 hours and the XRD recorded, Fig. S3. Analysis of the (002) peaks obtained for a drying temperature of 180°C shows that the distance between the GO sheets is 0.349 nm, 0.400 nm, 0.410 nm and 0.433 nm for GO, 67 mg GO mixed with 1 mmol TPA, 67 mg GO mixed with 1.3 mmol TOP and 67 mg GO mixed with 1 mmol TOP + 1.3 mmol TPA, respectively. The increased distance between the GO layers in the mixed system suggests that the combination of P containing surfactants can more readily penetrate the space between the GO layers.

Gas adsorption studies indicate specific surface areas (S_{BET}) of $PGO_{1TPA+1.3TOP,\ 800}$, $PGO_{1TPA,\ 800}$ and $PGO_{1.3TOP,\ 800}$ and $PGO_{7TPA,800}$ are 99.5 $m^2\ g^{-1}$, 113 $m^2\ g^{-1}$ and 295.7 $m^2\ g^{-1}$ and 132.6 $m^2\ g^{-1}$ with total pore volume (V_t) of 0.13 $cm^3\ g^{-1}$, 0.11 $cm^3\ g^{-1}$ and 1.27 $cm^3\ g^{-1}$ and 0.14 $cm^3\ g^{-1}$, respectively (see Fig. S4). The high specific surface area observed when TOP is used as a P source suggests that this surfactant is able to act as both a P-doping agent and better separate the graphene layer. The scanning electron microscopy (SEM) images of the microstructure of the PGO samples are displayed in Fig. S5-S8.

The percentage of O present in the PGO samples with low percentages of P are significantly lower than the amount of oxygen present in the initial GO indicating that TBP, TOP and TPA all act as strong reducing agents when annealing is performed at high temperature in an inert atmosphere. When the amount of P source employed in the synthesis, and hence the reducing power, is increased to increase P-doping, the amount of oxygen in the product also increases suggesting P-O bonds are present in the final material. High-resolution P2p and O1s XPS spectra were employed to probe the surface chemistry of the as-prepared PGO samples, see Fig. 1(b, c) and Fig. S9-S10. The P2p spectrum of $PGO_{1TPA+1.3TOP,800}$ can be deconvoluted into three peaks that are assigned to P-C (I), P=O/P-O-P (II) and P-O (III)[15, 16]. The O1s XPS spectra indicate that the as-prepared PGO contains bridging oxygen, -O- and P-O-H bonding (II, III). The O1s XPS spectrum also shows a peak at 531.4 eV which can be assigned to either C=O and/or P=O (I)[17-19] and the peak at 534.6eV is due to absorbed H_2O and O_2 (IV).

Measurements of the change of ratio between the intensity of the Raman G band peak, due to in plane motion of the sp^2 carbons, and the Raman D band peak, a result of out of plane vibrations, was employed to determine the change in defect density on doping. Raman spectra, measured using a 514 nm laser source, of GO, $PGO_{1TPA+1.3TOP,\ 800}$, $PGO_{1TPA,\ 800}$ and $PGO_{1.3TOP,\ 800}$ are displayed in Fig. 1d. An increase in the I_D:I_G ratio is apparent upon P-doping indicating that the reaction leads to an increase in the defect density in the 2D material. Raman spectra and I_D:I_G ratios for all as-prepared samples are shown in Fig. S11 and Table S5, respectively. In all cases an increase in defect density is observed upon P-doping. The full width at half maximum (FWHM) of the G band of $PGO_{1TPA+1.3TOP,800}$ is 54 cm^{-1}, smaller than GO (66.5 cm^{-1}). Change in FWHM indicates that the P doping stiffens G-mode phonons[20], consistent with increased charge carrier concentration. The PGO samples all show a downshifted G-mode compared with GO, suggesting π–p* conjugation due to the formation of P-C bond[21] and weakening of the bonds. The FWHM of the 2D band of PGO is larger than that of GO (see Fig. S11d) and the 2D-mode feature is upshifted after doping. The shift of the 2D mode and the scattered line width on P doping suggests that PGO is hole-doped[22]. Raman mapping of the I_D, I_G and $I_{D/G}$ peak intensities, Fig. 1e, indicates a uniform distribution of defects post P doping[20, 23].

The Selected Area Electron Diffraction (SAED) pattern measured in High-resolution Transmission Electron Microscopy (HRTEM) of $PGO_{1TPA+1.3TOP,\ 800}$, Fig. 1f, shows no long range order in the annealed material (see SAED in Fig. S12). The elemental mapping of $PGO_{1TPA+1.3TOP,\ 800}$ demonstrates that the P is uniformly distributed on the surface (see Fig. S13). The atomic force microscopy (AFM) image of $PGO_{1TPA+1.3TOP,\ 800}$ and corresponding line profiles are depicted in Fig. 1g and 1h. The AFM gives a range of material thicknesses between 2.34 and 5.03 nm, given the distance between GO layers is approximately 1 nm[24] the estimated num-

ber of layers in the as-prepared P doped materials is 2 to 5.

Charge Storage in PGO. The as-prepared PGO samples display quasi-rectangular CV curves, even at a scan rate of 5 V s^{-1} (Fig. 2a) and triangular shaped charge-discharge curves in the potential range 0.0 to -0.5 V (Fig. S14-S17). Control experiments indicate that the electrochemical characteristics of current collector in the working electrolyte and Au substrate contribute negligibly to the measured responses. The specific capacitance of the PGO tested at both 2 A g^{-1} and 3 A g^{-1} increases with the atomic % of P in the material (Fig. 2b). The sample with the highest P content, 10.19%, displays capacitances of 132.4 F g^{-1} and 95.7 F g^{-1} at 2 A g^{-1} and 10 A g^{-1}, exhibiting an energy density of 3.3 Wh kg^{-1} at a power density of 500 W kg^{-1} and an energy density of 2.5 Wh kg^{-1} at a power density of 2.5 KW kg^{-1} respectively. The increase in P content enhances the energy density from 0.72 to 4.6 Wh kg^{-1} at 500 W kg^{-1} of the sample with P content of 0.55% and 10.19%, see Ragone plot in Fig. S17d. The highly P doped samples, 10.19% and 7.77%, deliver promising cycling performance (see Fig. S18-S19). $PGO_{7TPA,\ 800}$ cycled at 10 A g^{-1} retains a specific capacitance of 90 F g^{-1} with a coulombic efficiency of 96.3% after 5000 galvanostatic charge/discharge cycles and $PGO_{1TPA+1.3TOP,\ 800}$ cycled at 15 A g^{-1} maintains 70.4 F g^{-1} with an efficiency of 82.7% after the same number of cycles. Compared to GO, the specific capacitance of the highly doped PGO is enhanced in terms of both magnitude and stability. The increased capacitance with P doping is also observed in the electrochemical impedance analysis of the electrodes, the Nyquist plot after 5 cycles of GO, $PGO_{1TPA+1.3TOP,\ 800}$ and $PGO_{1TPA,\ 800}$ are shown in figure 2(c) and the bode plots in figure S20. Nyquist and Bode plots after 1000 cycles for the same samples are displayed in figure S20. The equivalent circuits used to fit the data are shown in figure S20 and the values of the elements that yield the best fit to the data points, solid lines in the figures, are provided in table S6. In addition to capacitive components of higher magnitude upon P doping the EIS data also points to two time constants for charging the electrode in the presence of P and only a single time constant for GO electrode. The increase in capacitance with increased P doping does not follow the change in the measured surface area with doping. To explain why addition of P to GO both increases the capacitance and results in two time constants in the EIS spectra, DFT calculations were undertaken.

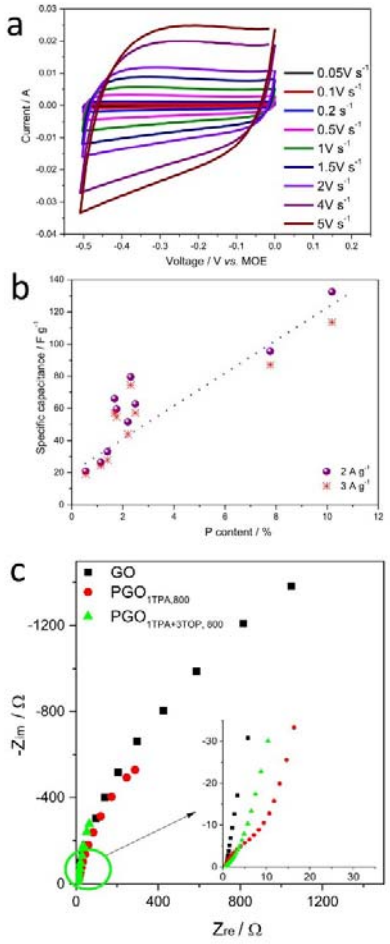

Fig. 2 Electrochemical characterization of P-doped graphene oxide. (a) Cyclic voltammetry curves of $PGO_{7TPA,\ 800}$ at different scan rates from 0.05 to 5 V s^{-1} in a voltage range of -0.5~0 V *vs.* MOE in 6M KOH electrolyte. (b) Relationship between the specific capacitance of PGO and P at.% content at current densities of 2 and 3 A g^{-1}. (c) Nyquist plot of GO, $PGO_{1TPA+1.3TOP,\ 800}$ and $PGO_{1TPA,\ 800}$ after 5 CV cycles at 0.5 V s^{-1}. The inset is magnified part of the circle.

Structure and bonding in PGO. To gain insight into the structure of PGO, we carried out DFT calculations of GO sheets with phosphorus defects (see Methods section for computational details). Two types of defects were studied: (i) phosphorus atoms which are adsorbed to the GO sheet and (ii) substitutional phosphorus atoms which replace carbon atoms in the basal plane of the GO sheet. To identify favourable low-energy configurations of P defects of type (i), we employed the following procedure: by adding epoxy and hydroxyl groups as well as vacancies at random positions to pristine graphene, an undoped GO sheet was prepared. Next, adsorbed P atoms are added at random positions and the whole structure is relaxed. We repeat

this procedure for many different initial configurations and sort the relaxed configurations according to their total energy.

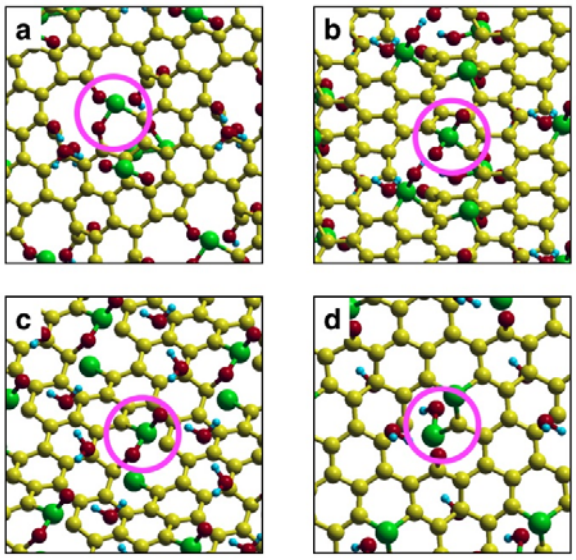

Fig. 3 Structure of P-doped graphene oxide. (a) and (b): Low-energy configurations of GO with adsorbed P atoms. (c) and (d): Low-energy configurations of GO with substitutional P atoms. Circles denote P atoms which are bonded to O atoms. The yellow is carbon, green is phosphorus, red is oxygen and blue is hydrogen atom.

Fig. 3 (a-b) show two low energy configurations resulting from this procedure. We observe two scenarios depending on the initial position of the P atom. If the P atom is initially in close vicinity (i.e. within 1 or 2 C-C bond lengths) of a vacancy or hole in the GO sheet, it will move to the vacancy or edge of the hole and pacify the available dangling bonds. Moreover, structures with particularly low energies exhibit P atoms at the edge of holes, which are bonded to one or more oxygen atoms. This explains our observation that samples with high P content also exhibit high O content, see Table 1, and is consistent with the XPS. Because of their large atomic radius, these bonded P atoms move above or below the GO basal plane and thereby enhance the specific surface area and specific capacitance of PGO. If, on the other hand, the P atom is initially located far from a vacancy or hole, it will form molecules with the oxygen and hydrogen atoms from epoxy and hydroxyl groups in its vicinity and desorb from the GO sheet. We also studied substitutional P defects in GO sheets. For this, we follow the same procedure as for the adsorbed P atoms, but instead of using a perfect graphene sheet as starting point, we employ a graphene sheet with several C atoms replaced by P atoms. After relaxation, we find that substitutional P atoms are stable and form low energy configurations when bonded to one or more oxygen atoms, see Fig. 3 (c-d).

Comparing the relative concentrations of adsorbed and substitutional P atoms in GO sheets is difficult, because each of the configurations obtained in the previous analysis features many different types of defects. To make progress, we compare the formation energies of adsorbed and substitutional P atoms in a graphene sheet with a single vacancy. Assuming that the substitutional P atom replaces a C atom located far from the vacancy and that the adsorbed P atom pacifies the dangling bonds at the vacancy site, we find that the formation energy of substitutional P atoms is higher than that of adsorbed P atoms by precisely the formation energy of a vacancy in graphene, which is of the order of 8 eV. This indicates that formation of adsorbed P atoms is favourable in graphene oxide.

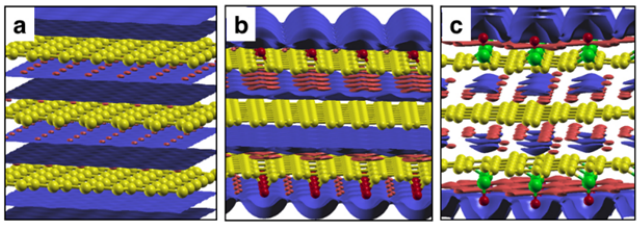

Fig. 4 Comparison of charge distribution in the electrolyte. (a) graphene, (b) graphene oxide and (c) PGO electrodes for an applied voltage of 1 eV with respect to the point of zero charge. Isosurfaces of positive and negative charge are blue and red, respectively. Yellow atoms are carbon, red atoms are oxygen and green atoms are phosphorus.

Electrochemical properties of PGO. To study the electrochemical properties of PGO, we carried out simulations of the PGO-electrolyte interface using the joint density-functional theory framework[25, 26]. Here, the aqueous electrolyte is described by a local dielectric function $\epsilon(r)$ and a local inverse Debye screening length $\kappa(r)$, whose spatial behaviour at the solid-liquid interface is determined by the electron density of the PGO electrode. To compute the capacitance of graphene oxide electrodes, we carried out calculations at an applied voltage of 1 V from the point of zero charge and determined the charge on the electrode.

From these calculations, we identified two mechanisms that contribute to the enhancement of the specific capacitance in PGO: i) increase of interlayer separation and ii) strong polarity of P-O groups. In particular, we observe that the capacitance of graphene trilayers approximately doubles as the interlayer separation is increased from the graphite value of 3.4 Angstrom to 4.7 Angstrom and then saturates. As the separation between the graphene sheets increases, electro-

lyte fills the space between the sheets and creates additional double layers which can store charge, see Fig. 4 (a). Comparing the charge distributions in the electrolyte for graphene, GO and PGO [see Fig. 4 (a)-(c)], we find that polar surface groups in GO and PGO significantly modify the structure of the electrochemical double layer. For graphene and graphene oxide, the negatively charged electrode induces a (mostly) positive charge distribution in the electrolyte. Surprisingly, for PGO we observe a thin layer of negative charge in the electrolyte adjacent to the negatively charged electrode followed by a layer of positive charge. We attribute this structure, which enhances the charge storage capability of PGO, to the strong polarity of the P-O groups. A Lowdin population analysis reveals that the P atom in PGO loses 1.6 electrons and therefore carries a large positive charge which attracts negative ions more strongly than the negatively charged graphene plane.

To conclude, highly phosphorus doped graphene oxide (PGO) was prepared by the thermal decomposition of P containing surfactants; TPA, TBP and TOP. The specific capacitance of the as-prepared samples increased with the amount of P incorporated in the graphene oxide layers. PGO with P at.% of 7.77% displayed specific gravimetric capacitances of 95.6 F g^{-1} and 72.4 F g^{-1} at 2 A g^{-1} and 10 A g^{-1}, and maintained 70.4 F g^{-1} with an efficiency of 82.7% after 5000 cycles at 15 A g^{-1}. DFT calculations show that phosphorus atoms prefer to adsorb to defects in the GO sheet rather than substitute for carbon atoms in the basal plane of the GO sheet. The doping of P atoms can improve the charge storage capability by increasing interlayer separation of GO and the strong polarity of P-O groups leading to specific adsorption of ions at the surface.

ASSOCIATED CONTENT

Supporting Information. More characterization results.

AUTHOR INFORMATION

Corresponding Author

jason.riley@imperial.ac.uk (Jason Riley)

Notes

The authors declare no competing interests.

ACKNOWLEDGMENT

We thank the President's Ph.D. Scholarship of Imperial College London, the Engineering and Physical Sciences Research Council (EPSRC, Grant: EP/L015277/1) and STFC Future Early Career Award for financial support. J. L. acknowledges support from the Thomas Young Center under Grant No. TYC-101. Via J. L.'s membership of the UK's HEC Materials Chemistry Consortium, which is funded by EPSRC (EP/L000202), this work used the ARCHER UK National Supercomputing Service. CM acknowledges the award of a Royal Society University Research Fellowship by the UK Royal Society and the support from the EPSRC through grants EP/K01658X/1, EP/K016792/1. V.G. Rocha would like to acknowledge the European Commission (FP7 Marie Curie Intra-European Fellowships GRAPES) and EPSRC grant EP/KO1658X/1.

REFERENCES

(1) Geim, A. K. Graphene: Status and Prospects. *Science* **2009**, *324*, 1530-1534.

(2) Li, D.; Kaner, R. B. Graphene-Based Materials. *Science* **2008**, *320*, 1170-1171.

(3) Long, J.; Xie, X.; Xu, J.; Gu, Q.; Chen, L.; Wang, X. Nitrogen-Doped Graphene Nanosheets as Metal-Free Catalysts for Aerobic Selective Oxidation of Benzylic Alcohols. *ACS Catal.* **2012**, *2*, 622-631.

(4) Chen, D.; Feng, H.; Li, J. Graphene oxide: preparation, functionalization, and electrochemical applications. *Chem. Rev.* **2012**, *112*, 6027-6053.

(5) Xu, B.; Yue, S.; Sui, Z.; Zhang, X.; Hou, S.; Cao, G.; Yang, Y. What is the choice for supercapacitors: graphene or graphene oxide? *Energ. Environ. Sci.* **2011**, *4*, 2826.

(6) Chen, Y.; Zhang, X.; Zhang, D.; Yu, P.; Ma, Y. High performance supercapacitors based on reduced graphene oxide in aqueous and ionic liquid electrolytes. *Carbon* **2011**, *49*, 573-580.

(7) Lin, Y.; Liu, F.; Casano, G.; Bhavsar, R.; Kinloch, I. A.; Derby, B. Pristine Graphene Aerogels by Room-Temperature Freeze Gelation. *Adv. Mater.* **2016**, *28*, 7993-8000.

(8) Wei, X.; Jiang, X.; Wei, J.; Gao, S. Functional Groups and Pore Size Distribution Do Matter to Hierarchically Porous Carbons as High-Rate-Performance Supercapacitors. *Chem. Mater.* **2016**, *28*, 445-458.

(9) Jeong, H. M.; Lee, J. W.; Shin, W. H.; Choi, Y. J.; Shin, H. J.; Kang, J. K.; Choi, J. W. Nitrogen-Doped Graphene for High-Performance Ultracapacitors and the Importance of Nitrogen-Doped Sites at Basal Planes. *Nano Lett.* **2011**, *11*, 2472-2477.

(10) Xu, X.; Sun, Z.; Chua, D. H. C.; Pan, L. Novel nitrogen doped graphene sponge with ultrahigh capacitive deionization performance. *Sci. Rep.* **2015**, *5*, 11225.

(11) Zhang, X.; Lu, Z.; Fu, Z.; Tang, Y.; Ma, D.; Yang, Z. The mechanisms of oxygen reduction reaction on phosphorus doped graphene: A first-principles study. *J. Power Sources* **2015**, *276*, 222-229.

(12) Zhang, C.; Mahmood, N.; Yin, H.; Liu, F.; Hou, Y. Synthesis of phosphorus-doped graphene and its multifunctional applications for oxygen reduction reaction and lithium ion batteries. *Adv. Mater.* **2013**, *25*, 4932-7.

(13) Some, S.; Kim, J.; Lee, K.; Kulkarni, A.; Yoon, Y.; Lee, S.; Kim, T.; Lee, H. Highly air-stable phosphorus-doped n-type graphene field-effect transistors. *Adv. Mater.* **2012**, *24*, 5481-6.

(14) Yang, D.-S.; Bhattacharjya, D.; Inamdar, S.; Park, J.; Yu, J.-S. Phosphorus-Doped Ordered Mesoporous Carbons with Different Lengths as Efficient Metal-Free Electrocatalysts for Oxygen Reduction Reaction in

Alkaline Media. *J. Am. Chem. Soc.* **2012**, *134*, 16127-16130.

(15) Wen, Y.; Wang, B.; Huang, C.; Wang, L.; Hulicova-Jurcakova, D. Synthesis of phosphorus-doped graphene and its wide potential window in aqueous supercapacitors. *Chemistry* **2015**, *21*, 80-85.

(16) Kannan, A. G.; Choudhury, N. R.; Dutta, N. K. Synthesis and characterization of methacrylate phospho-silicate hybrid for thin film applications. *Polymer* **2007**, *48*, 7078-7086.

(17) Shih, P. Y.; Yung, S. W.; Chin, T. S. FTIR and XPS studies of P2O5–Na2O–CuO glasses. *J. Non-cryst. Solids* **1999**, *244*, 211-222.

(18) Bagri, A.; Mattevi, C.; Acik, M.; Chabal, Y. J.; Chhowalla, M.; Shenoy, V. B. Structural evolution during the reduction of chemically derived graphene oxide. *Nat Chem* **2010**, *2*, 581-587.

(19) Mattevi, C.; Eda, G.; Agnoli, S.; Miller, S.; Mkhoyan, K. A.; Celik, O.; Mastrogiovanni, D.; Granozzi, G.; Garfunkel, E.; Chhowalla, M. Evolution of Electrical, Chemical, and Structural Properties of Transparent and Conducting Chemically Derived Graphene Thin Films. *Adv. Funct. Mater.* **2009**, *19*, 2577-2583.

(20) Berciaud, S.; Ryu, S.; Brus, L. E.; Heinz, T. F. Probing the Intrinsic Properties of Exfoliated Graphene: Raman Spectroscopy of Free-Standing Monolayers. *Nano Lett.* **2009**, *9*, 346-352.

(21) Zhang, C.; Wang, X.; Liang, Q.; Liu, X.; Weng, Q.; Liu, J.; Yang, Y.; Dai, Z.; Ding, K.; Bando, Y., et al. Amorphous Phosphorus/Nitrogen-Doped Graphene Paper for Ultrastable Sodium-Ion Batteries. *Nano Lett* **2016**, *16*, 2054-60.

(22) Das, A.; Pisana, S.; Chakraborty, B.; Piscanec, S.; Saha, S. K.; Waghmare, U. V.; Novoselov, K. S.; Krishnamurthy, H. R.; Geim, A. K.; Ferrari, A. C., et al. Monitoring dopants by Raman scattering in an electrochemically top-gated graphene transistor. *Nat. Nanotech.* **2008**, *3*, 210-215.

(23) Cançado, L. G.; Jorio, A.; Ferreira, E. H. M.; Stavale, F.; Achete, C. A.; Capaz, R. B.; Moutinho, M. V. O.; Lombardo, A.; Kulmala, T. S.; Ferrari, A. C. Quantifying Defects in Graphene via Raman Spectroscopy at Different Excitation Energies. *Nano Lett.* **2011**, *11*, 3190-3196.

(24) Park, S.; Ruoff, R. S. Chemical methods for the production of graphenes. *Nat. Nanotech.* **2009**, *4*, 217-224.

(25) Letchworth-Weaver, K.; Arias, T. A. Joint density functional theory of the electrode-electrolyte interface: Application to fixed electrode potentials, interfacial capacitances, and potentials of zero charge. *Phys. Rev. B.* **2012**, *86*, 075140.

(26) Petrosyan, S. A.; Rigos, A. A.; Arias, T. A. Joint Density-Functional Theory: Ab Initio Study of Cr2O3 Surface Chemistry in Solution. *J. Phys. Chem. B* **2005**, *109*, 15436-15444.